Metascience in Aerospace

Metascience in Aerospace, 2(1): 1–14.
DOI: 10.3934/mina.2025001
Received date: 07 February 2025
Revised date: 21 March 2025
Accepted date: 03 April 2025
Published date: 21 April 2025

https://www.aimspress.com/journal/mina

Research article

For electrified aircraft propulsion, SiC MOSFET inverter design with power redundancy in both escape event and failure

Simon Kim[1], Donghyun Lee[2], Byunggil Kwak[3] and Myeonghyo Kim[3]

[1] Infineon Technologies Korea, System application engineer team, Seoul Korea
[2] Hanwha Systems, Power control team, YoungIn, Korea
[3] Hanwha Aerospace, Advanced Technology R&D Center, Seongnam, Korea

* **Correspondence:** Email: Simon.Kim@infineon.com.

Abstract: To reduce carbon dioxide emissions, electrified aircraft propulsion has been extensively studied worldwide. Among electrified aircraft, urban air mobility features short-range flying times. Both fully electric and hybrid types have been developed, undergoing field tests and awaiting commercial service induction. This paper describes a virtual electrical aircraft propulsion system designed as a 600 kW-rated aviation system for five passengers and one pilot, with some luggage, simulating a real flight. The propulsion system is powered by batteries and motors, comprising 12 distributed electric propulsion (DEP) systems. Each DEP inverter circuit is a two-level, three-phase inverter. A silicon carbide (SiC) metal–oxide–semiconductor field-effect transistor (MOSFET) module and an isolation gate driver Integrated Circuit (IC) are used to evaluate this inverter system. Through a virtual power profile, power redundancy is analyzed under normal conditions and unplanned worst-case scenarios. For a planned trajectory, the system's power profile is assessed during the takeoff, cruise, and landing phases. The DC-link voltage discharged is also reviewed for these flight stages. In some cases, due to external conditions, a quick escape motion during the cruise phase requires the propulsion system to operate at maximum power for a specific duration. In such unplanned events, flight time extends, leading to greater DC-link voltage discharge compared with a planned trajectory. To calculate power loss, switching losses are measured using a demo power board. These measurement results are used in loss simulation instead of datasheet values. Each DEP's output power value is derived from the system's virtual profile, and each DEP inverter's power loss is calculated through measurement-based simulation. Maximum power and current are evaluated as critical conditions in each virtual profile. Through loss and thermal simulations, the power redundancy of the proposed DEP inverter system is validated for use in electric propulsion systems.

Keywords: Distributed electric propulsion (DEP) system; electrified aircraft propulsion (EAP); silicon carbide (SiC) metal-oxide-semiconductor field-effect transistor (MOSFET); virtual aviation systems; virtual power profile; power redundancy; failure redundancy

1. Introduction

To achieve net-zero emissions, the electrification of various applications has been a key focus for many years. One key area of interest has been the electrification of aircraft, which has been widely studied. The topic of more-electric aircraft (MAE) and all-electric aircraft (AEA) with megawatt power, with a focus on distributed propulsion architecture, was discussed in [1], together with the all-electric N3-X aircraft from NASA. In [2], a power generation method was proposed and verified through MATLAB/Simulink. In [3], a commercial aircraft using systems with AC currents was studied and reviewed. In [4], current problems in fully electrified aircraft (FEAs) were defined through a mathematical and mechanical approach. The ratio between the horizontal flight range of an aircraft with constant mass and the horizontal flight range of an aircraft with variable mass was determined. To increase the flying time, a hybrid electric aircraft (HEA) was proposed. In [5], the benefits, e.g., energy saving, of hybrid electric propulsion systems were reviewed, although at a reduced range relative to the conventional gas turbine-powered aircraft. In [6], a fuel-cell hybrid electric aircraft (FCHEV) and other solutions were compared during a one-hour general flight mission profile.

Several topologies for MEA, HEA, and AEA were reviewed and studied in [7]. In [8], different types of converter and inverter topologies—two-level, three-level, and five-level circuit topologies—for aircraft propulsion applications were reviewed and checked for efficiency and failure in time with power density. In [9], multilevel inverters (MLI) for aviation applications were studied and evaluated with two-level circuit topologies. In [10], the failure correlation between the DC-link voltage and altitude due to cosmic radiation was evaluated. A proposed variable DC-link voltage profile was introduced and simulated. Regarding megawatt (MW) charging, the charging technology for electric aircraft was reviewed in [11], together with the latest developments and future trends in electric aviation. In [12], higher power levels in transportation electrification at the MW scale were discussed. Key technologies enabling transportation electrification systems of MW scale, such as power electronic converters, battery chemistry, high power connectors, and smart grid integration technologies, as well as the standards and challenges within the transportation industry, were explored. Regarding motor designs, in [13], electric motor technologies enabling electrically propelled aircraft, including their current type and prototype, were reviewed and studied. In [14], the wound-rotor synchronous machine (WRSM) for aircraft hybrid-electric propulsion systems was introduced, and a control strategy was proposed for failure events.

Regarding design parameters and tools, the performance of a light aircraft with a mechanical engine was compared to an electrically propelled aircraft with a similar capacity using computational tools. In [15], researchers provided insights into the performance and handling characteristics of the aircraft, highlighting both the strengths and potential areas for improvement in the designs. In [16], some prototypes classified as long-range, medium-short-range, and urban transportation were introduced, and design parameters were reviewed. In [17], case studies for electrified aircraft propulsion (EAP) were discussed, and a cost analysis of the EAP aircraft concepts was done. In [18], based on research by the Center for High-Electrical Technologies for Aircraft (CHEETA), aircraft

concepts with several propulsion configurations were compared in distributed electric aircraft propulsion systems. The optimization of the fan and motor was proposed. In [19], researchers evaluated how to verify the system's performance and compatibility with related standards in a laboratory setting, through functional checks. In [20], the use of large waste thermal energy was discussed, and the current state-of-the-art, objectives, system design architecture, and remaining technical challenges in system formulation were introduced. In [21], researchers introduced a kilowatt test platform for electrified aircraft propulsion systems with a battery profile in which the DC-link voltage was reduced from 800 to 516 V in 1700 seconds. In [22], the history of UAM was discussed. It also introduced the aviation marketplace ecosystem and provided some recommendations for future research on sustainability, social and economic impacts, and airspace integration. In [23], flying cars and eVTOLs' weight and power information were shared and studied. For the virtual aircraft system discussed in this paper, a 560 kW-rated electric aviation system for five passengers performs the "lift + cruise flying process", and its power range is referred to as the target power. In [24], for a DEP with multiple propellers and motors, two three-phase inverters with SiC MOSFETs were investigated with different control strategies. In [25], the maximum power used for takeoff and landing was discussed. The power in cruise mode was shown to be one-third of the maximum power. [26] proved that after applying a recursive pulse current to a battery, comparing the measurement result and the R-C modeling shows both voltage drop and recovery characteristics. In [27], the DC link was derived from the research results on a unit battery's voltage profile with the voltage's state of charge (SOA). [28] discussed the measured voltage mission profile of the lithium-ion battery cell unit in an electrical vertical takeoff and landing (eVTOL) vehicle, specifically the Airbus Vahana, detailing its voltage-drop and recovery characteristics. Throughout the entire flight duration, the battery cell voltage decreased from 4.2 to 3.1 V. In [29], the system-level DC-link voltage was derived from the unit cell voltage [28] and evaluated under both normal operating conditions and unexpected events.

The virtual aircraft discussed in this paper is set as a short-range urban transportation. For reduced weight, base-less SiC MOSFET modules are used as the two-level, three-phase DEP inverter. In the virtual profile, the discharged DC-link voltage, the DEP's output power, the output current, and the sustained number of DEP units are described in the flight time. Different system power levels are set for the takeoff, cruise, and landing phases. The virtual profile is set and modified for a normal, planned trajectory and for a changed trajectory caused by an unexpected event or failure. The DEP inverter's critical operation is tested for these different virtual profiles. Through measurement-based loss simulation and thermal simulation, the power capability of the DEP system is checked, and the power redundancy of the virtual aircraft is evaluated.

2. A virtual electric aircraft with DEP system

Similarly to [23], our virtual system's total output power is set to 600 kW; as a result, the power of one side wing is 300 kW. The DEP system is comprised of 12 inverter units, motors, and propellers. This virtual system is battery-operated, and the full-charge voltage is 800 V. The battery can discharge to around 500 V after takeoff, cruise, and landing phases with an unwanted event. The rated power of each inverter is 50 kW, as listed in Table 1. Considering the overload rate, each DEP inverter's maximum power is set to 75 kW. The failure redundancy is set to 1. The virtual system's configuration is shown in Figure 1.

First, the virtual system is evaluated in a virtual profile with the normal planned trajectory, as shown in Figure 2. For 1 minute, the takeoff process is operated. The system propulsion's output power during this phase is 300 kW in both right- and left-wing propulsion systems. During the cruise phase, a relatively low power compared to takeoff is set: the system propulsion's output power is set to 100 kW for each wing. During landing, the system propulsion's output power is set to 300 kW in both right- and left-wing propulsion systems. Cruise time is defined as 20 minutes, excluding both takeoff and landing phases. In all three flight phases, the DC-link voltage is decreased. Particularly during the takeoff and landing phases, a steep drop in voltage is noted. After takeoff, the system propulsion's output power lowers from 300 to 100 kW for each wing's propulsion system, and the rapidly decreasing DC-link voltage recovers from 690 to 747 V_{dc}. During the cruise phase, one side wing's propulsion power is reduced to one-third of the output propulsion's power during takeoff, and the DC-link voltage decreases from 747 to 695 V_{dc}. During landing, the DC-link voltage drops from 690 to 581 V_{dc}. When all propulsion systems are stopped, the DC-link voltage is recovered around 690 V_{dc}, because there is no more output power.

For the unwanted external event, a disturbance caused by a flock of birds was considered in the virtual profile. During the cruise phase, at 1000 seconds, the virtual electric propulsion system performs a quick escape motion. The output power for one wing increases to 400 kW for 20 seconds. The power then reduces to 200 kW for 30 seconds due to the changed trajectory, as shown in Figure 3. Due to this event, the DC-link voltage drops from 706 to 630 V_{dc}. Due to this quick escape and altered trajectory for 50 seconds, the cruise time increases by around 5 minutes. For the landing process, 300 kW output power is required for each side wing's propulsion system.

Table 1. Virtual power system.

Item	Value	Unit
System output power (P_{OUT})	600	kW
Number of DEP system	12	Unit
Max. voltage in DC link	800	V_{dc}
Min. voltage in DC link	500	V_{dc}
Each DEP's rated power	50	kW
Overload rate	50	%
Failure redundancy	1	Pieces

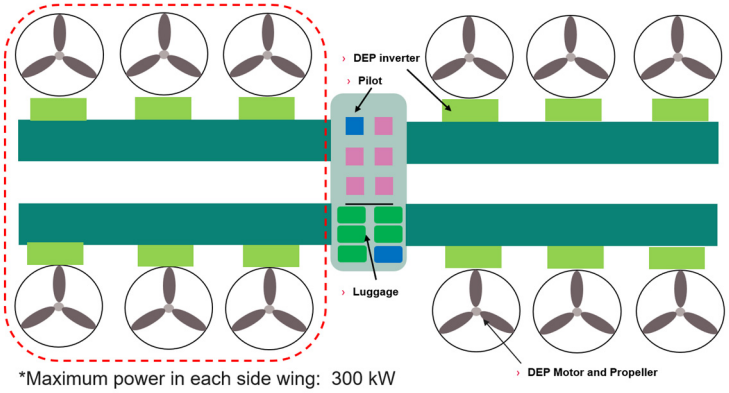

Figure 1. Virtual electrical aircraft with 12 DEP systems with a maximum power of 300 kW per side wing.

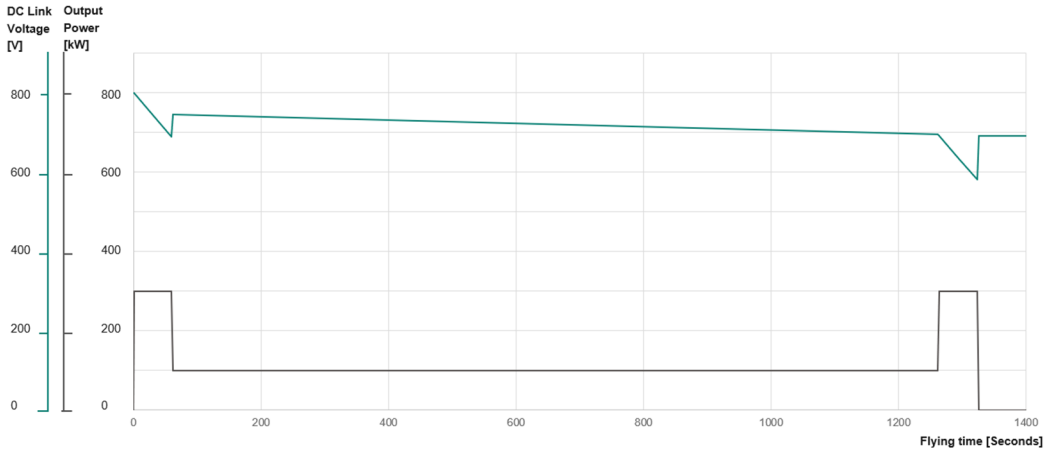

Figure 2. Virtual profile with no unexpected event and failure.

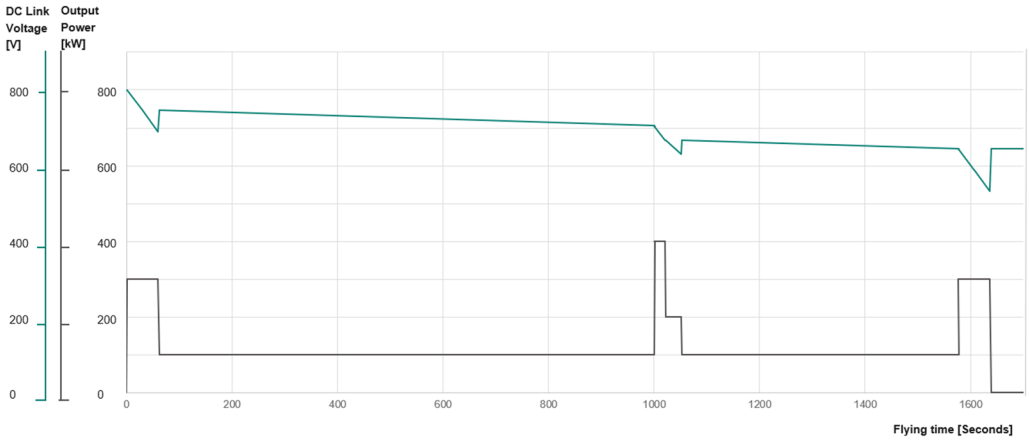

Figure 3. Virtual profile with an escape unplanned event.

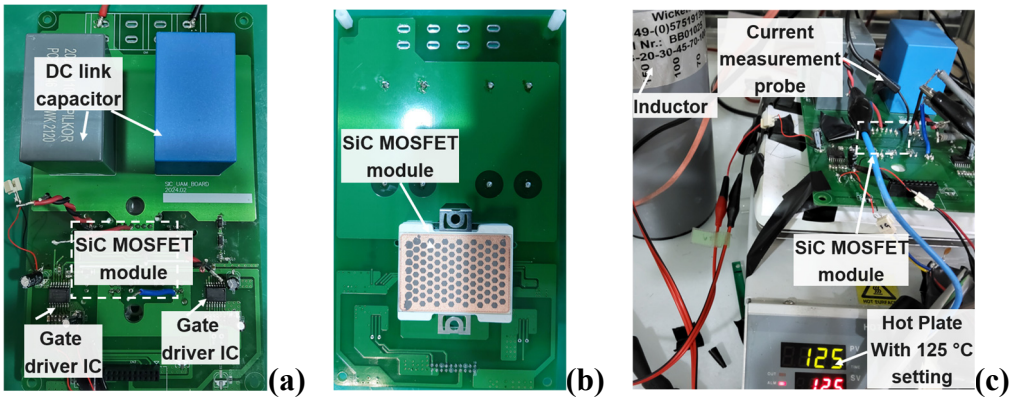

Figure 4. Demo board with double-pulse test. (a) Top view of the demo board with half-bridge circuit of SiC MOSFETs and isolation gate driver IC. (b) Bottom view of the demo board. (c) Double-pulse test with the inductor and hot plate.

3. Measurement-based simulation for power loss and thermal performance in a DEP system

For each DEP inverter system, the proposed module is F4-8MR12W2M1H (H-bridge circuit, 8 mΩ SiC MOSFET). This is a base-less module used as a half-bridge circuit and these three modules constitute a 2-level 3-phase inverter. Its equivalent electrical capability is a 1200 V 4 mΩ SiC MOSFET chip and a half-bridge circuit. 1ED3322MC12N is used as the 1-channel isolated gate driver IC, and its electric current capacity is 6 A peak current at turn-on and −8.5 A peak current at turn-off. A real system's switching loss is larger than the datasheet value because of the Printed Circuit Board (PCB) design's stray inductance. Therefore, the E_{on} and E_{off} are measured through a double-pulse input test with a demo board composed of a SiC MOSFET module and a gate driver IC, as shown in Figure 4 (a) and (b). Figure 4 (c) and Figure 5 show the measurement setup with a hot plate at 125 °C. The measurement circuit and E_{off} result are also shown. The first pulse lets the output current reach the target current, and then the E_{off} loss is measured at the falling edge of the second pulse. E_{on} loss is measured at the rising edge of the second pulse. Figure 5 shows the measured value of E_{off}. For this measurement, 345 μH inductor is used as load inductor (L1). For maximum charging DC-link voltage, 800 V_{dc} is applied to the capacitor (C1) in the circuit. As gate voltage, 15 V is applied to the secondary side of the gate driver IC, without minus voltage. The measured E_{off} loss is 2.27 mJ at the applied current, 100 A. The measurements are taken at both 25 °C and 125 °C. A hot plate with a surface temperature of 125 °C is used to take the measurement at 125 °C. The target SiC MOSFET is put on this surface, and E_{on} and E_{off} are measured.

Then, measured E_{on} and E_{off} are then used to simulate power loss, instead of the datasheet value, as they reflect a more real system. PLECS is used to simulate the loss, as shown in Figure 6, using a sine pulse with a sinusoidal pulse-width modulation (SPWM). The power loss is calculated to fix the heatsink temperature to 90 °C.

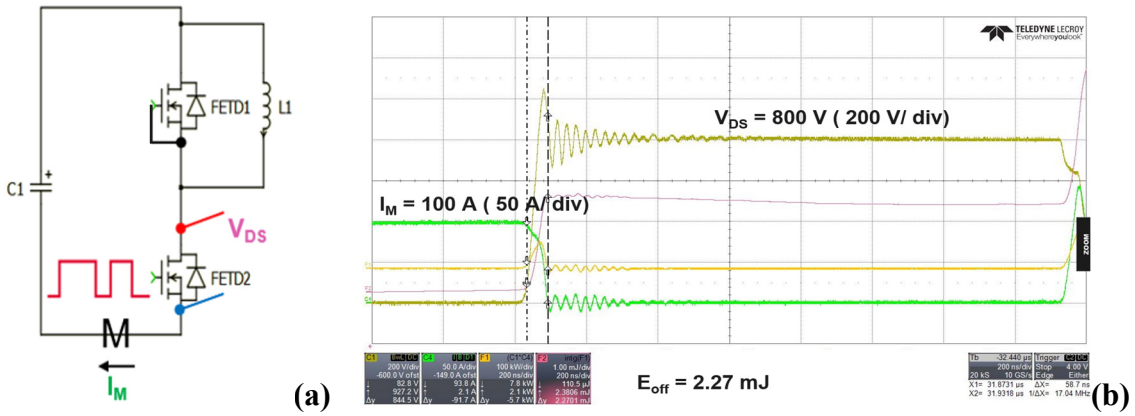

Figure 5. E_{off} measurement by double pulses. (a) Measurement circuit. (b) Measurement result for E_{off} = 2.27 mJ at 100 A.

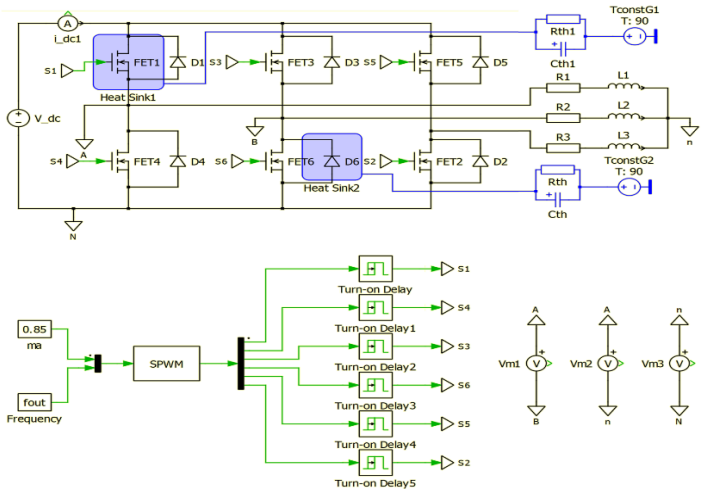

Figure 6. Loss simulation for two-level, three-phase inverter with measurement data.

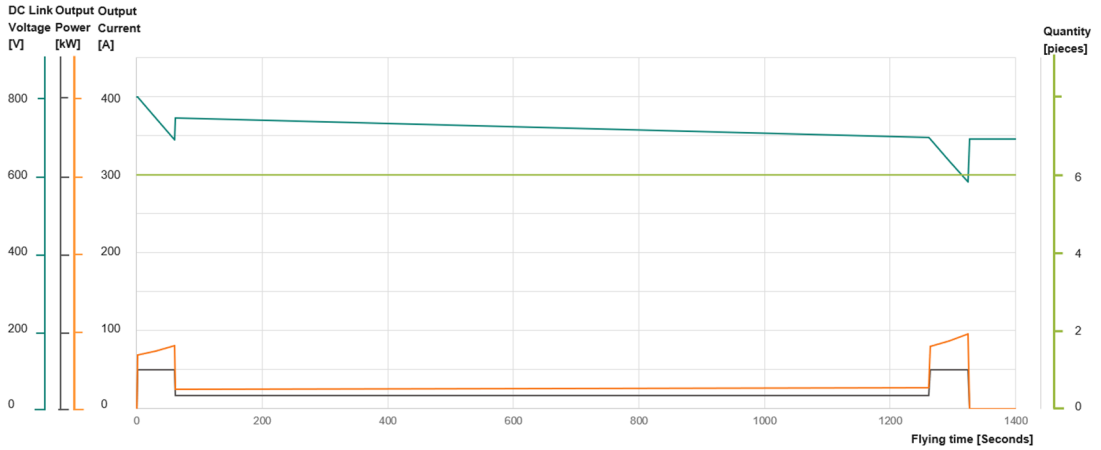

Figure 7. DEP profile with a normal planned trajectory.

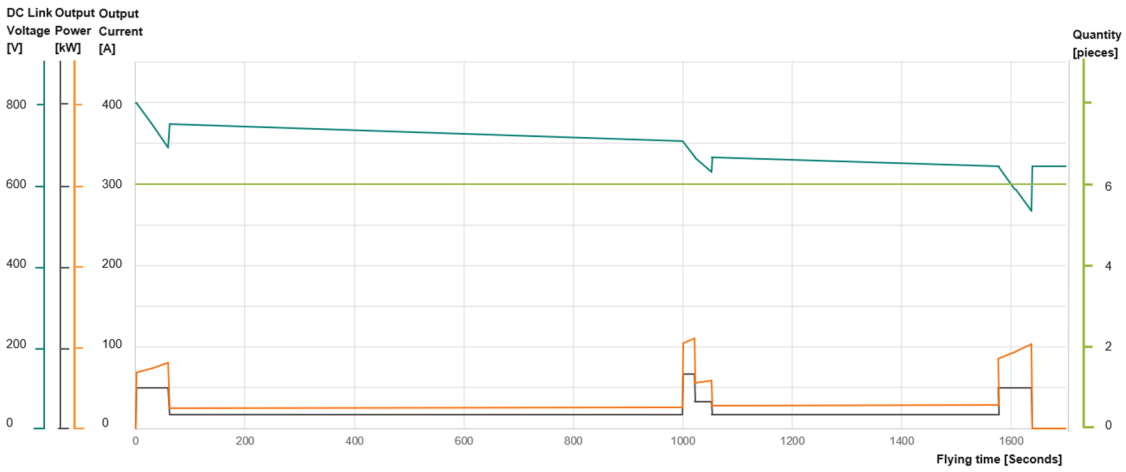

Figure 8. DEP profile with an escape unplanned event.

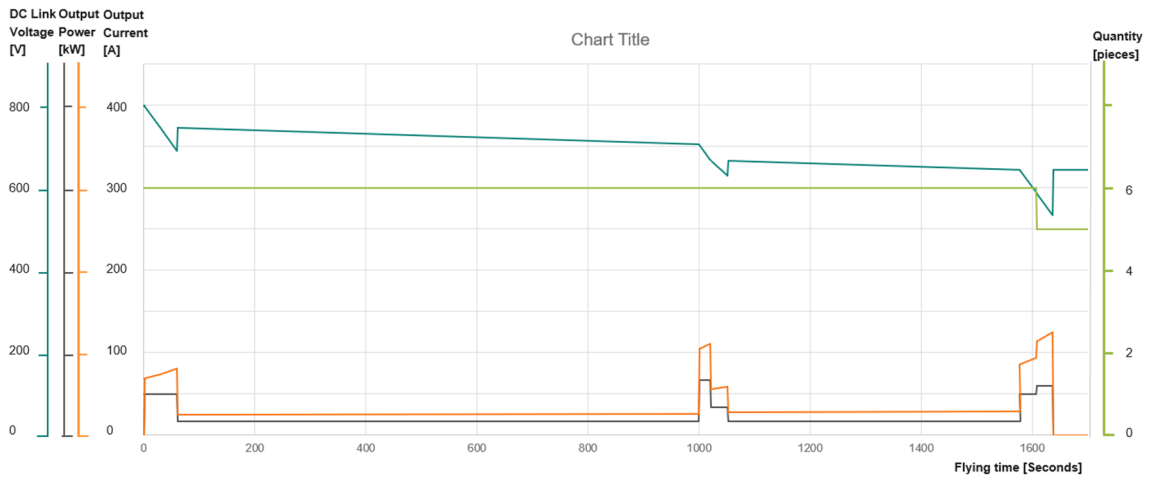

Figure 9. DEP profile with an escape unplanned event and one failure.

First, the DEP system is evaluated in a normal planned trajectory without any unwanted event. At the system level, the same output propulsion power in both takeoff and landing phases is reviewed, as shown in Figure 2. Each DEP system is assumed to share the system power at the same rate. In the cruise phase, DC-link voltage decreases. Even though the output propulsion power is the same during both takeoff and landing phases, each DEP's output current during the landing phase is higher than during takeoff due to decreased DC-link voltage, as shown in Figure 7. In this case, DEP's maximum output current during takeoff is 80.4 A. However, the maximum output current during landing is 95.4 A because the DC-link voltage discharges from 690 to 581 V_{dc}.

Second, the DEP system is evaluated during an unwanted event. The scenario consists of a flock of birds due to which the virtual electrical aviation system has to perform an escape motion with maximum power. For this quick escape motion, 400 kW is set as the output power of one side wing's propulsion system. This power is distributed within the six DEP inverters on that side wing, i.e., each DEP system's output power is 67 kW. During this time, the output current is 110.7 A, as shown in Figure 8. Due to the changed trajectory, the flying time is extended. Each DEP's output current during the landing process is 103.9 A with a DC-link voltage of 534 V_{dc}.

Third, the DEP system is evaluated not only with the escape motion but also with one failure. The failure is considered during the landing process. When a propeller and the motor are stuck due to an unknown mechanical failure, the remaining five DEP unit systems must redistribute the wing propulsion's total output power. In this scenario, the output power of one DEP inverter increases from 50 to 60 kW. At the same time, its output current is also increased from 103.9 to 124.6 A. Now, the DEP system's output power of 60 kW is lower than its output power during the quick escape motion, which is 67 kW. This means that the output current of one DEP inverter during the landing process with one failure is higher than its output current during the quick escape motion in the cruise process. This is shown in Figure 9 in orange.

These different cases must be evaluated through thermal simulation to check the power capability of each DEP inverter. In the virtual profile review, some maximum power and current scenarios were checked for these critical cases.

As shown in Table 2, one DEP inverter's output power during the quick escape process is 67 kW, and its output current is 110.7 A with a DC-link voltage of 668 V. In this case, by measuring E_{on} and

E_{off} data, PLECS simulation is done. The loss of each SiC MOSFET is 67.9 W, and its body diode's loss is 14.2 W. The total loss of half-bridge module is 164.3 W.

Thermal simulation is conducted using the online simulation tool Mersen R-TOOLS MAXX. For the 67 kW-rated output power during the quick escape motion, the module's power loss from measurement-based simulation is 164.3 W. As mentioned in the previous section, the F4-8MR12W2M1H module is used as a half-bridge circuit with 1ED3322MC12N as the isolated gate driver IC. For each module's thermal simulation, a heatsink with dimensions 92 mm × 92 mm × 35mm is used separately. The indirect forced air cooling is set to 110 cubic foot/minute (CFM = 0.0519142195 m^3/s), which is equivalent to a 92 mm fan's cooling capability. The loss calculated by measurement-based simulation is applied to the direct copper bonding (DCB) dimension in the F4-8MR12W2M1H module. The surface temperature of the heatsink obtained through thermal simulation is 65.7 °C, as shown in Figure 10.

Table 2. Loss of SiC MOSFET in each DEP system by its output power and current during a quick escape process.

Item	Value	Unit
P_{OUT} in one DEP at quick escape	67	kW
Min. DC-link voltage at quick escape	668	V
Output current at quick escape	110.7	A
SiC MOSFET's loss	67.9	W
SiC MOSFET's body diode loss	14.2	W
Half-bridge module's total loss	164.3	W

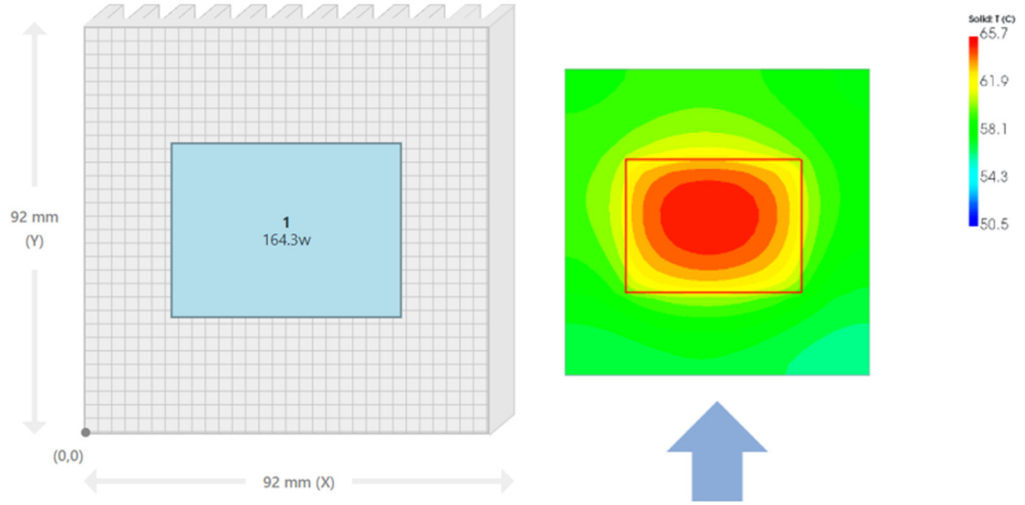

Figure 10. Loss simulation results with one DEP's output power at 67 kW by quick escape motion.

As listed in Table 3, one DEP inverter's output power during the landing process with one failure is 60 kW, and its output current is 124.6 A with a DC-link voltage of 534 V. As per the measurement-based loss simulation, the MOSFET's loss in the SiC MOSFET (P_M) is 75.8 W, and the body diode's loss is 16.6 W. The total loss in the half-bridge module is 184.9 W.

For thermal simulation, the same heatsink and forced air cooling are used. The total loss of one module by measurement-based simulation, i.e., 184.9 W, is applied on the module's DCB dimension. The calculated surface temperature of the heatsink (T_H) is 68.9 °C, as shown in Figure 11. Based on

the datasheet values, R_{thJH} is derived as 0.394 K/W. From these values, the estimated junction temperature is calculated using the following equation [28]:

$$T_{VJ} = R_{thJH} * P_M + T_H \quad (1)$$

The calculated T_{VJ} is 98.8°C ($R_{thJH} \times P_M + T_H = 0.394 \times 75.8 + 68.9$ °C). This junction temperature provides enough thermal margin, as the module's maximum operating temperature while switching is 175 °C. Considering the margin, even if the maximum operating temperature is 150 °C, a thermal margin of over 50 °C is available.

Table 3. Output power and current during the landing phase with one failure.

Item	Value	Unit
P_{OUT} in one DEP at landing with one failure	60	kW
Min. DC-link voltage at landing	534	V
Output current at landing	124.6	A
SiC MOSFET's loss	75.8	W
SiC MOSFET's body diode loss	16.6	W
Half-bridge module's total loss	184.9	W

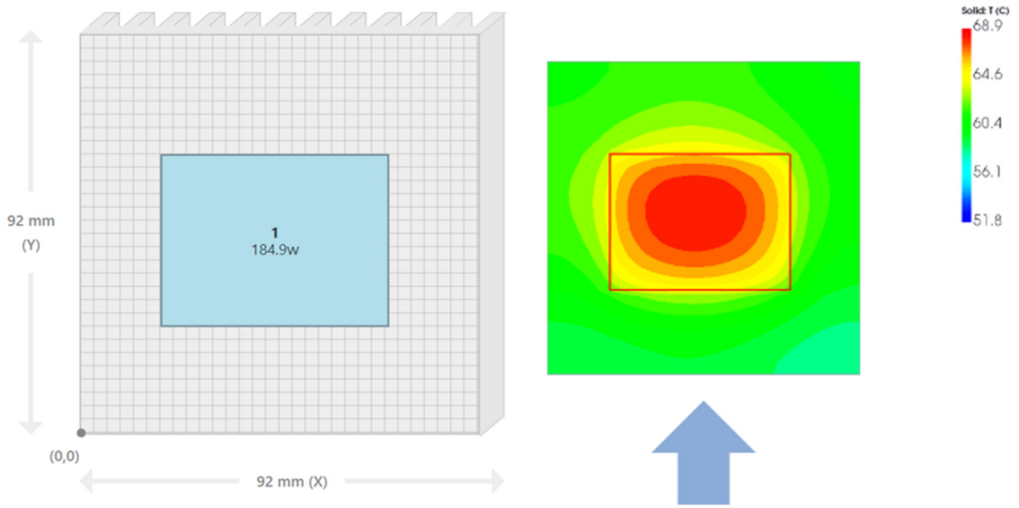

Figure 11. DEP's output power of 60 kW during the landing phase with one failure.

For a more critical condition, two failures are considered. Here, the wing's propulsion system's 300 kW is distributed among the remaining four DEP units during the landing process. Now, one DEP inverter's output power during landing with two failures is 75 kW, and its output current is 155.8 A with a DC-link voltage of 534 V. From the measurement-based simulation, the SiC MOSFET's loss (P_M) obtained is 113.2 W, and its body diode's loss is 22.5 W. The half-bridge module's total loss is 271.3 W.

For the thermal simulation, the same heatsink and forced air cooling are used. The total loss of one module by measurement-based simulation, i.e., 271.3 W, is applied on the module's DCB dimension. The calculated surface temperature of the heatsink (T_H) is 82.4 °C, as shown in Figure 12. The R_{thJH} is 0.394 K/W. From these values, the estimated junction temperature (T_{VJ}) is calculated using Eq (1). The T_{VJ} is 127.0 °C ($R_{thJH} \times P_M + T_H = 0.394 \times 113.2 + 82.4$ °C). In [31], the qualifying

temperature range for an electric component's thermal margin in an electric propulsion is given as ± 21 °C.

Table 4. Output power and current during the landing phase with two failures.

Item	Value	Unit
P_{OUT} in one DEP at landing with two failures	75	kW
Min. DC-link voltage at landing	534	V
Output current at landing	155.8	A
SiC MOSFET's loss	113.2	W
SiC MOSFET's body diode loss	22.5	W
Half-bridge module's total loss	271.3	W

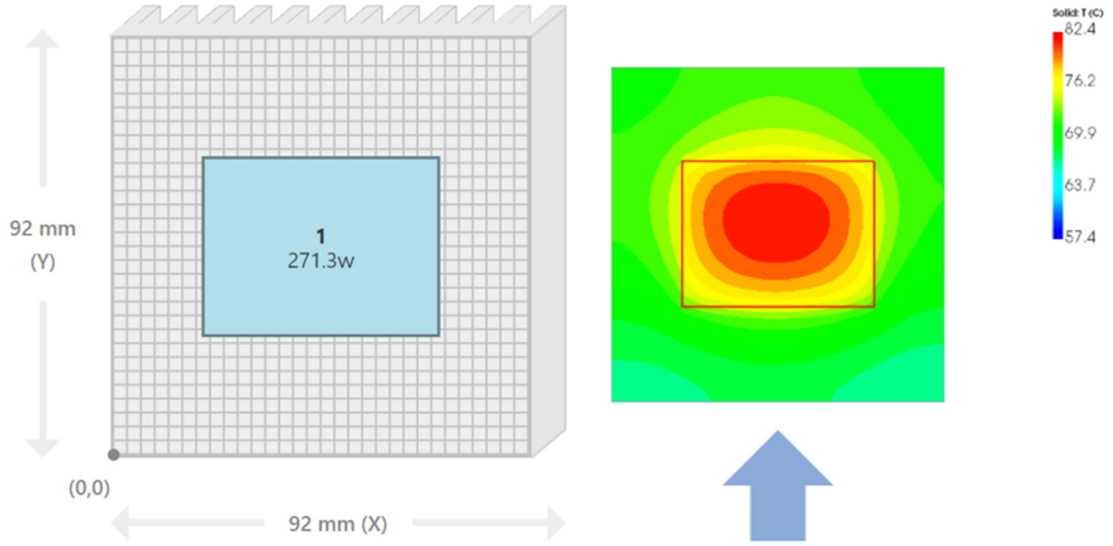

Figure 12. DEP's output power of 75 kW during the landing phase with two failures.

Even with two failures during the landing phase, a thermal margin of 23 °C will be available during operation if the virtual junction temperature is limited to 150 °C.

4. Conclusions

For this study, only measurement data and simulation results were used. The virtual profile of a battery-operated, 600 kW-rated electric aircraft with one pilot, five passengers, and some luggage was evaluated. This virtual electrical aviation system was composed by 12 DEP units. The power redundancy of each operational DEP was checked using virtual profiles that included different scenarios, namely a quick escape motion caused by external events as well as failures in one or two DEP systems. Each DEP inverter comprised a two-level, three-phase circuit. E_{on} and E_{off} were measured through a double-pulse test using a demo board with F4-8MR12W2M1H as the half-bridge SiC MOSFET circuit and 1ED3322MC12N as the isolated gate driver IC. The measured values, instead of datasheet values, were then used to simulate power loss. A profile with two failures during the landing phase after an escape motion was analyzed as the most critical operating scenario.

To evaluate the DEP's power redundancy, the thermal performance of the half-bridge circuit was checked using a heatsink of dimensions 92 mm × 92 mm × 35 mm and indirect forced cooling. The

results showed that the estimated junction temperature of the SiC MOSFET was in the safe thermal zone with adequate thermal margins.

Author contributions

All authors contributed to the study conception. Simon wrote the first draft of paper, Donghyun did investigation, Byunggil reviewed and Myeonghyo did validation.

Use of AI tools declaration

The authors declare they have not used Artificial Intelligence (AI) tools in the creation of this article.

Acknowledgments

I received support from several colleagues. Special thanks to Ainhoa Puyadena Mier, Technical Marketing Engineer in Germany for discussing this topic with me in detail.

Conflict of Interest

The authors declare no conflicts of interest.

References

1. Barzkar A, Ghassemi M (2022) Components of Electrical Power Systems in More and All-Electric Aircraft: A Review. *In 2022 IEEE Transactions on Transportation Electrification,* 8: 4037–4053. https://doi.org/10.1109/TTE.2022.3174362
2. Bai G, Bozhko S, Yang T, et al. (2023) Power Flow Analysis of Advanced Power Generation Centre for More Electric Aircraft. *In 2023 IEEE Transportation Electrification Conference and Expo, Asia-Pacific (ITEC Asia-Pacific).* https://doi.org/10.1109/ITECAsia-Pacific59272.2023.10372301
3. Madonna V, Giangrande P, Galea M (2018) Electrical Power Generation in Aircraft: Review, Challenges, and Opportunities. *In 2018 IEEE Transactions on Transportation Electrification,* 4.
4. Dukhnovskiy DA (2020) Formation of the Area of Possible Existence of Electrified Airplanes. *In 2020 New Trends in Aviation Development (NTAD),* 2020: 49–53. https://doi.org/10.1109/NTAD51447.2020.9379118
5. Decerio DP, Hall DK (2022) Benefits of Parallel Hybrid Electric Propulsion for Transport Aircraft. *In IEEE Transactions on Transportation Electrification*, 8: 4054–4066. https://doi.org/10.1109/TTE.2022.3193622
6. Li S, Zhao P, Gu C, et al. (2024) Hybrid Power System Topology and Energy Management Scheme Design for Hydrogen-Powered Aircraft. *In 2024 IEEE Transactions on Smart Grid,* 15: 1201–1212. https://doi.org/10.1109/TSG.2023.3292088.
7. Buticchi G, Wheeler P, Boroyevich D (2023) The More-Electric Aircraft and Beyond. *In 2023 Proceedings of the IEEE,* 111: 356–370. https://doi.org/10.1109/JPROC.2022.3152995

8. Luckett B, He JB (2023) Genetic Algorithm Enabled Multi-Objective Design Optimization of Power Converters for Electric Aircraft Propulsion. *In 2023 IEEE Energy Conversion Congress and Exposition (ECCE),* 1836–1842. https://doi.org/10.1109/ECCE53617.2023.10361949
9. Wang D, Hemming S, Yang Y, et al (2024) Multilevel Inverters for Electric Aircraft Applications: Current Status and Future Trends. *In 2024 IEEE Transactions on Transportation Electrification,* 10: 3258–3282. https://doi.org/10.1109/TTE.2023.3296284
10. Fauth L, Ebersberger J, Cao Y, et al. (2023) Advantages of a Variable Board Supply Voltage in All-Electric Aircraft with Regard to Cosmic Radiation Induced Failures. *In 2023 IEEE International Conference on Electrical Systems for Aircraft, Railway, Ship Propulsion and Road Vehicles & International Transportation Electrification Conference (ESARS-ITEC),* 2023: 1–6. https://doi.org/10.1109/ESARS-ITEC57127.2023.10114811
11. Liang Y, Mouli GRC, Bauer P (2024) Charging Technology for Electric Aircraft: State of the Art, Trends, and Challenges. *In 2024 IEEE Transactions on Transportation Electrification,* 10: 6761–6788. https://doi.org/10.1109/TTE.2023.3333536
12. Mirza AY (2024) A Review of Key Technology Enablers and Challenges in Megawatt Scale On-road and Off-road Transportation Electrification. *In 2024 IEEE Transportation Electrification Conference and Expo (ITEC),* 2024: 1–5. https://doi.org/10.1109/ITEC60657.2024.10599054
13. Molina MJ, Graffeo F, Vaschetto S, et al. (2024) Application and Performance Trends of Electric Motors for Aircraft Propulsion. *In 2024 IEEE Transportation Electrification Conference and Expo (ITEC),* 2024: 1–8. https://doi.org/10.1109/ITEC60657.2024.10598961
14. Lu J, Zhang Z, Li J, et al. (2024) A Single-Stage Control Strategy of Wound-Rotor Synchronous Starter Generator Under Excitation Failure Conditions for Hybrid-Electric Propulsion Aircraft Application. *In 2024 IEEE Transactions on Transportation Electrification,* 10: 5368–5378. https://doi.org/10.1109/TTE.2023.3329981
15. Furmanek R, ŠkráŠek R, Filochowski B, et al. (2023) Implementation of Alternative Aircraft Evaluation Techniques to Assess Electrical Aircraft Performance. *In 2023 IEEE International Conference on Electrical Systems for Aircraft, Railway, Ship Propulsion and Road Vehicles & International Transportation Electrification Conference (ESARS-ITEC),* 2023: 1–4. https://doi.org/10.1109/ESARS-ITEC57127.2023.10114854
16. Delogu G, Porru M, Serpi A (2021) A Brief Overview on Commercial Aircraft Electrification: Limits and Future Trends. *In 2021 IEEE Vehicle Power and Propulsion Conference (VPPC),* 2021: 1–5. https://doi.org/10.1109/VPPC53923.2021.9699191
17. Ty VM, Nathaniel JB, Zachary JF, et al. (2021) Results for an Electrified Aircraft Propulsion Design Exploration. *In 2021 AIAA/IEEE Electric Aircraft Technologies Symposium (EATS),* 2021: 1–16. https://doi.org/10.23919/EATS52162.2021.9704848
18. Chandel D, Reband JD, Hall DK, et al. (2023) Fan and Motor Co-Optimization for a Distributed Electric Aircraft Propulsion System. *In 2023 IEEE Transactions on Transportation Electrification,* 9. https://doi.org/10.1109/TTE.2022.3204202
19. SaĞirkaya H (2023) Design and Verification of Aircraft Electrical Power System. *In 2023 IEEE International Conference on Electrical Systems for Aircraft, Railway, Ship Propulsion and Road Vehicles & International Transportation Electrification Conference (ESARS-ITEC),* 2023: 1–6. https://doi.org/10.1109/ESARS-ITEC57127.2023.10114894

20. Hendricks TJ, Tarau C, Dyson RW (2021) Hybrid Electric Aircraft Thermal Management: Now, New Visions and Future Concepts and Formulation. *In 20th IEEE Intersociety Conference on Thermal and Thermomechanical Phenomena in Electronic Systems (iTherm),* 2021: 467–476. https://doi.org/10.1109/ITherm51669.2021.9503205
21. Arenas O, McQueen M, Robertson D, et al. (2022) Implementation of a 200 kW Adaptable Testing Platform for Experimental Research in Electrification of Aircraft Propulsion. *In 2022 IEEE Transportation Electrification Conference & Expo (ITEC),* 2022: 856–861. https://doi.org/10.1109/ITEC53557.2022.9813971
22. Cohen AP, Shaheen SA, Farrar EM (2021) Urban Air Mobility: History, Ecosystem, Market Potential, and Challenges. *In 2021 IEEE Transactions on Intelligent Transportation Systems,* 22: 6074–6087. https://doi.org/10.1109/TITS.2021.3082767
23. Swaminathan N, Reddy SRP, RajaShekara K, et al. (2022) Flying Cars and eVTOLs—Technology Advancements, Powertrain Architectures, and Design. *In 2022 IEEE Transactions on Transportation Electrification,* 8: 4105–4117. https://doi.org/10.1109/TTE.2022.3172960
24. Fischer D, Rohn R, Mallwitz R (2023) Design Approach of an Integrated SiC-Inverter for an Electrical Aircraft. *In ESARS- ITEC. 2023 IEEE International Conference on Electrical Systems for Aircraft, Railway, Ship Propulsion and Road Vehicles & International Transportation Electrification Conference (ESARS-ITEC),* 2023: 1–6.
25. Yang XG, Liu T, Ge S, et al. (2021) Challenges and key requirements of batteries for electric vertical takeoff and landing aircraft. *Joule* 5: 1644–1659.
26. Kulkarni C, Hogge E, Quach CC (2018) Remaining Flying Time Prediction Implementing Battery Prognostics Framework for Electric UAV's. *In 2018 Engineering.*
27. Liu W, Deng Z, Hu X (2022) Investing the Electrothermal Behavior of eVTOL batteries in Urban Air Mobility applications. *In 25th Intelligent Transportation Systems,* 8–12.
28. Mitici M, Hennink B, Pavel M, et al. (2023) Prognostics for Lithium-ion batteries for electric vertical take-off and landing aircraft using data-driven machine learning. *In 2023 Energy and AI,* 12: 100233. https://doi.org/10.1016/j.egyai.2023.100233
29. Kim S, Lee D, Mier AP, et al. (2024) A SiC MOSFET propulsion inverter design with power redundancy, considering unwanted events, for electrical aircrafts. *In 2024 IEEE Transportation Electrification Conference and Expo (ITEC),* 2024: 1–6. https://doi.org/10.1109/ITEC60657.2024.10599039
30. Infineon application note AN2011-05 (2011) AN2011-05 industrial IGBT modules explanation of technical information. 18.
31. Wilhite JM, Borer NK, Frederick M (2024) Thermal Environments and Margin Guidelines for NASA's X-57 "Maxwell" Flight Demonstrator. *In AIAA Scitech 2024 Forum*, 2024: 1475. https://doi.org/10.2514/6.2024-1475

AIMS Press